Jurnal Tribologi 41 (2024) 144-161

Jurnal Tribologi
Website : jurnaltribologi.mytribos.org
e-issn: 2289-7232

Effect of anodizing voltage on surface and physical properties of CNTs incorporated aluminium oxide films

Aflah A Aziz [1], Md Shuhazlly Mamat [1], Mohd Mustafa Awang Kechik [1], Kar Fei Chan [1], Muhammad Izzat Muktar [1], Noor Ayuma Mat Tahir [2], Shahira Liza Kamis [2], Yazid Yaakob [1,3*]

[1] Department of Physics, Faculty of Science, Universiti Putra Malaysia, 43400 UPM Serdang, Selangor, MALAYSIA.
[2] Tribology and Precision Machining i-Kohza (TriPreM), Malaysia-Japan International Institute of Technology, Universiti Teknologi Malaysia, Jalan Sultan Yahya Petra, 54100 Kuala Lumpur, MALAYSIA.
[3] Halal Products Research Institute, Universiti Putra Malaysia, 43400 UPM Serdang, Selangor, MALAYSIA.
*Corresponding author: yazidakob@upm.edu.my

KEYWORDS

Carbon nanotubes
Anodizing voltage
Anodic aluminium oxide
Surface properties
Hardness

ABSTRACT

In this study, the surface characteristics of CNTs/Al_2O_3 films growth from Al alloy were investigated at different anodizing voltage. The samples were anodized in sulphuric acid containing CNTs as electrolyte with the voltage ranging from 5 V to 15 V. Surface morphology and crystal structure were observed with SEM and XRD, while the microhardness was analysed via Vickers hardness tester. The XRD spectra revealed that bare aluminium, AAO and AAO-CNTs composed orthorhombic and γ-Al_2O_3. The surface topography was examined with 3D Optical Profiler, and the findings showed that higher anodizing voltage leads to higher surface roughness (5.71 µm) and pores dimension (w: 43.69 µm and d: 39.63 µm). By adding CNTs, it can reduce surface roughness to 4.80 µm by 16% with pore dimension (w: 37.79 µm and d: 33.78 µm). It can be supported by SEM-EDX showing that enhancement of CNTs into AAO is believed to reduce the porosity. The Vickers hardness of AAO-CNTs showed the highest value which is 210.40 HV compared to the bare aluminium alloy (130.50 Hv) and AAO (198.60 Hv), as CNTs filled in the porosity of oxide layer. This finding provides an additional knowledge incorporating CNTs into aluminum oxide through anodizing technique.

Received 6 November 2023; received in revised form 3 February 2024; accepted 14 April 2024.
To cite this article: Aziz et al., (2024). Effect of anodizing voltage on surface and physical properties of CNTs incorporated aluminium oxide films. Jurnal Tribologi 41, pp.144-161.

1.0 INTRODUCTION

High-strength aluminium (Al) and its alloys remain widely used in various industrial fields including automotive, aerospace, and transportation parts. Al alloy has much been preferred due to its lightweight, good corrosion resistance, and exceptional mechanical strength (Dervishi et al., 2022a). However, the inherent drawbacks of Al alloys like low hardness, poor tribological, and interfacial mechanical properties remain challenges to be utilized in extensive applications (Li et al., 2014). This included the Al alloys having higher friction coefficients ranging from 0.4-0.8 and wear rate measurement from 10^{-4}-10^{-5} mm^3/m during dry sliding conditions (D. Zhang et al., 2014). It is due to the the intermetallic compounds such as Mg, Cu, Cr, and Mn found in Al alloys are susceptible to fracture as these impurities act as robust sites for crack initiation and affect the interfacial properties (Ebhota & Jen, 2018; Yang et al., 2022). Regarding that, researchers and engineers have employed a wide range of surface treatment methods over the past few decades to improve typically substandard mechanical and tribological properties of Al alloys. Several approaches such as chemical vapor deposition (CVD), thermal spraying, physical vapor deposition (PVD), and ion beam assisted deposition have been applied to improve the surface protection of Al alloy (Li et al., 2014). However, most of the aforementioned approaches mentioned before entailing high temperatures during processing, which may potentially degrade the coating or the substrate. Hence, making them less ideal for aluminium coatings (Li et al., 2014). Therefore, to counter these problems and prolong the surface protection of Al alloy, this work is subjected to use anodizing method to produce aluminium oxide coating. Anodizing is one of the promising surface-modification techniques and is cost-effective in manufacturing, particularly for Al alloys (Ayuma et al., 2022). Composite oxide film coatings are produced through an electrochemical process in which aluminium undergoes oxidation, leading to the formation of a stable oxide layer on the Al alloy surface (Brudzisz et al., 2021). This process is conducted under specific anodizing conditions, involving several parameters such as anodizing voltage ranging at 19-25 V (Brzózka et al., 2020) and 15-25 V (Sulka, 2008). Additionally, the process incorporates the utilization of electrolytes with varying concentrations, such as 3.65 M sulphuric acid (Mohamad et al., 2020; Rawian et al., 2023), oxalic acid, and phosphoric acid within the range of 0.22 to 0.45 M and 0.4 to 3.10 M (Sulka, 2008). When Al is used as the anode in an electrolyte solution containing phosphoric, oxalic, sulphuric, and chromic acid it endures a process that results in the formation of an anodic film. This film comprises two distinct layers: a barrier-type ultra-thin and a thicker porous oxide layer (Dervishi et al., 2022a). The formed oxide layer improves surface properties like hardness, wear resistance, and corrosion resistance besides permitting aesthetic decoration (Ayuma et al., 2022; Mohamad et al., 2020; Remešová et al., 2020). However, while anodization can enhance the surface properties of Al alloys, it has been reported that coatings produced through anodization on the top layer present cracks, voids, and numerous pores as a result of the applied potentials (Mohamad et al., 2020). Consequently, the anodic oxide layer is insufficient to protect aluminium alloy in a corrosive environment. If fractures of film loss occur in the anodic oxide layer as a result of heat, mechanical stress, or high applied voltage, corrosive substances may penetrate the alumina. Thus, leading to significant damage to the base material (Al alloy) (Yamamoto and Nonaka, 2022). At potentials higher than 5 V, transverse cracks and voids are observed in the porous nanostructure tin oxide films and too high voltage will damage the oxide layer (Dervishi et al., 2022a). Raising the voltage disrupts the anodic aluminium oxide arrangement and leads to an increased number of defects in the oxide film (Stêpniowski et al., 2012). Li et al. (2014) revealed that as the cathodic voltage increased, the coating thickness significantly improved, and it exhibited a more compact structure. In the past few decades,

researchers have conducted numerous studies using reinforcement fillers in composite oxide films. A study by Lv et al. (2009) had used graphite as filler in alumina coatings indicated higher performance coating prior to corrosion resistance. Rawian et al. (2023) conducted a study where they successfully improved the surface quality of aluminium oxide incorporating diamond-like carbon, which effectively reduced the presence of microcracks. As a result of this enhancement, the microhardness trend increased up to 240.944 Hv (Rawian et al., 2023). Previous research by Abebe et al. (2022) used zirconium dioxide as ceramic reinforcement. The study indicated that the mechanical strength of the composite film was increased as a result of a strong bond between matrix and reinforcement particles. All the findings mentioned before showed that the incorporation of fillers brings improvement in the surface properties of aluminium oxide and increases the hardness significantly.

Regarding that, the main objective of this research is to initially grow anodic aluminium oxide (AAO) with a porous structure, which is subsequently filled with carbon nanotubes (CNTs). CNTs are regarded as highly promising reinforcement materials in composite materials featuring in metal for their impressive mechanical properties, large aspect ratio, and low density (Jagannatham, Sankaran, & Prathap, 2015). CNTs have garnered popularity due to their exceptionally outstanding properties, such as high thermal conductivity, excellent mechanical, and electrical properties (Gul et al., 2023). The exceptional rigidity and strength of CNTs originate from the covalent of sp^2 bonding between carbon-carbon (C-C) configuration (Naqi et al., 2019). Several research studies have shown the successful reinforcement of CNTs in a ceramic and metal matrix. Chan et al. (2021) reported that a low amount of CNTs can strengthen ceramic matrix including fracture toughness, density, thermal conductivity, and wear resistance. A study conducted by Li et al. (2014) used CNTs as reinforcement particles played an important role in the reduction of pore size. According to a study by Sabouri & Mousavi Khoei (2018), the incorporation of MWCNTs has enhanced the density of coating through the micropores. Alishahi et al. (2012) reported that CNTs incorporated into the coating increased the hardness of the Ni-P composite and contributed to an improvement in the nanocrystalline phase. The mechanical properties of Al-Cu composites increased by 154% as a result of the uniform distribution of CNTs and load transfer from the matrix to the reinforcement (Jagannatham, Sankaran, & Haridoss, 2015). The microhardness of the coating escalated from 730 Hv to 785 Hv, corresponding to an increase in CNTs content through the electroless co-deposition technique (Gul et al., 2023). Other findings from T. Zhang et al. (2009) revealed that the inclusion of CNTs into aluminium oxide via the CVD technique resulted in an augmentation of up to 8.4% in hardness and 21.1% in toughness compared to monolithic aluminium oxide. To the best of the author's knowledge, there is limited research on AAO reinforced CNTs by anodization. Hence, in this work, the objective of this study is to elucidate the growth mechanism and microhardness of the CNTs-AAO at different anodizing voltage.

2.0 MATERIALS AND METHODS

2.1. Raw Materials

Aluminium alloy AA2017-T4 disk with 25 mm diameter (Misumi Malaysia Sdn. Bhd), MWCNTs (≥98% carbon, Sigma-Aldrich), sulphuric acid (H_2SO_4 (95-98%), R&M Chemicals), and copper sheet (99.9% pure solid copper with 200 mm x 200 mm x 0.5 mm) were purchased.

2.2. Surface Preparation

The anodizing experiment was conducted using AA2017-T4 as anode. The AA2017 alloy rod was first prepared by segmenting the rod into individual pieces. Each piece had a constant thickness of 4 mm and the middle of the disk was drilled to form a 4 mm hole. AA2017 disk was then ground using silicon carbide (SiC) papers: 800w, 1000w, 1200w, 1500w, and 2000w to remove surface impurities. The copper plate was utilized as cathode and its dimension was cut to 40 mm x 60 mm. The disk and copper plate were then cleaned ultrasonically using an ethanol bath for 10 minutes and subsequently soaked in deionized water to clear the ethanol solution out.

2.3. Anodization Treatment Process

The anodization process is performed directly using a direct current (DC) power supply (Maisheng MS-305D 0-30V 10A). Figure 1 depicts the schematic diagram of the anodizing setup. Concentrated sulphuric acid (H_2SO_4) received was diluted with deionized water to prepare 20 wt% of H_2SO_4 electrolyte. The electrolyte used in the anodizing process was initially maintained at the ambient conditions under 23°C and the electrolyte temperature variations were monitored using an IR-750 infrared thermometer Amprobe, AMB-50, IR-750-EUR. 0.5 g/L of as-received CNTs was weighed and mixed with electrolyte. The CNTs-electrolyte was then sonicated for approximately 10 minutes to ensure homogenous and well dispersion of CNTs before being used in the anodizing process. The anodizing was performed for 60 minutes at different anodizing voltage of 5 V, 10 V, 12 V, and 15 V. Lastly, the anodized sample was cleaned with distilled water to remove excess electrolyte and dried with a blower before being characterized. The anodic aluminium oxide (AA0) and anodic aluminium oxide-CNTs composite (AAO-CNTs) samples were synthesized as a comparison. The anodizing parameters, anodizing voltage and sample abbreviations are summarized in Table 1 and Table 2.

Table 1: Anodizing parameters.

Cathode	Copper plate
Anode	AA2017
Current density (A/dm²)	15
Temperature	Room temperature
Electrolyte	20 wt% H_2SO_4
Anodizing time (min)	60
Concentration of CNTs (g/L)	0.5

Table 2: Anodizing voltage and sample abbreviations.

Manipulated Variables	
Voltage (V)	5, 10, 12, 15
Sample Abbreviations	
Anodic aluminium oxide	AAO
Anodic aluminium oxide-CNTs composite	AAO-CNTs

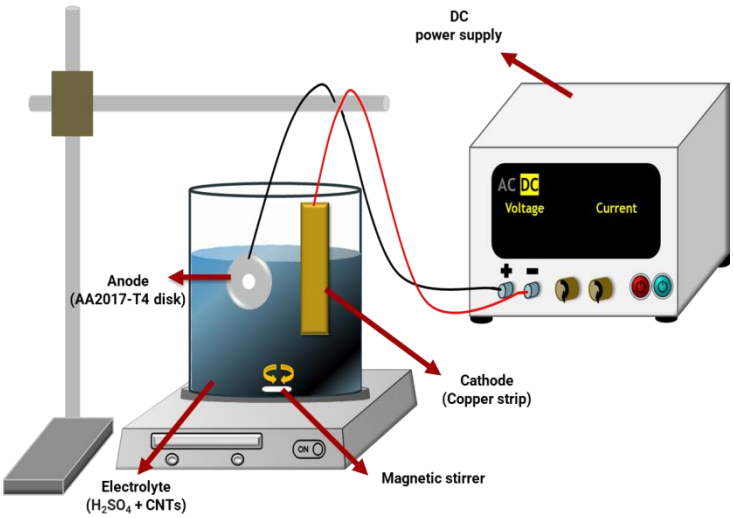

Figure 1: Schematic diagram of anodization set-up.

2.4 Surface Characterization

The phase composition analysis of AAO and AAO-CNTs were determined by X-ray Diffratometer (XRD, PW 3040/60 MPD X'pert Pro Panalytical, Philips, Netherlands). Scanning Electron Microscopy with EDX (SEM, JEOL JSM IT-100, United States) was used to examine the surface morphology and elemental composition. Surface topography was analyzed by using a Digital Microscope (HIROX Kh-8700, USA). The calculated area and porosity measurement of AAO and AAO-CNTs was determined using the pixel-to-size converter in the ImageJ software. The microhardness of AAO was analysed by using Micro Vickers Hardness (HM-G30 Shimadzu Corporation, Japan). The sample was loaded with 0.1 HV (980.7 mN) for 10 s duration time.

3.0 RESULTS AND DISCUSSION

3.1. Voltage and Temperature Change during Anodization

The behavior of AAO and AAO-CNTs influenced by anodizing voltage and temperature is depicted in Figure 2. At the beginning of the anodizing process, the voltage recorded was 5 V, 10 V, 12 V, and 15 V and the initial temperature of the electrolyte was found to be approximately 26.6 ℃, 25.9℃, 23.9 ℃, and 25.5 ℃ for anodized samples, respectively. In contrast with AAO-CNTs, the temperature was recorded around 31.6 ℃, 32 ℃, 31.4 ℃, and 30 ℃, as a result of the sonication effect before anodization process. This sonification step ensured the thorough mixing and dispersion of CNTs, thus achieving more uniform and well-distributed particles. It has been observed that the utilization of ultrasonic treatment results in the generating of heat (Asadi et al., 2019).

However, as time passed, the voltage started to decrease and the temperature increased rapidly. To fill in the porosity, the incorporation of CNTs is vital in this work. The voltage drop is faster when CNTs are present in the system compared to anodizing without CNTs. When CNTs are in contact with an anode, the electrons can move faster and flow more easily with minimal resistance, thus promoting the growth of the oxide layer. Generally, CNTs are a good electrical

conductivity. When CNTs are dispersed in electrolyte during anodization, they serve as conductive pathways. These characteristics allowed the electrolyte to conduct electricity with minimal resistance. Resulting that, the anodization voltage is reduced rapidly as the thicker oxide layer has higher resistance. This is in agreement with previous research that used graphite as reinforcement in the anodizing process (Mohamad et al., 2020). In addition, higher electrical conductivity will increase the electrolyte's temperature due to the ionization process. Herein, it can increase the chemical anodic dissolution in forming AAO. Based on the graphs, it shows that the temperature of AAO-CNTs is decreased than AAO. It is suggested that the high thermal conductivity of CNTs may aid in helping the heat to dissipate rapidly, thereby potentially reducing the overall temperature of the electrolyte. The inclusion of CNTs in the oxide facilitates efficient heat dissipation from the electrolyte due to CNTs have excellent thermal conductivity (Da Silva Tousch et al., 2023; Hwang & Chung, 2018).

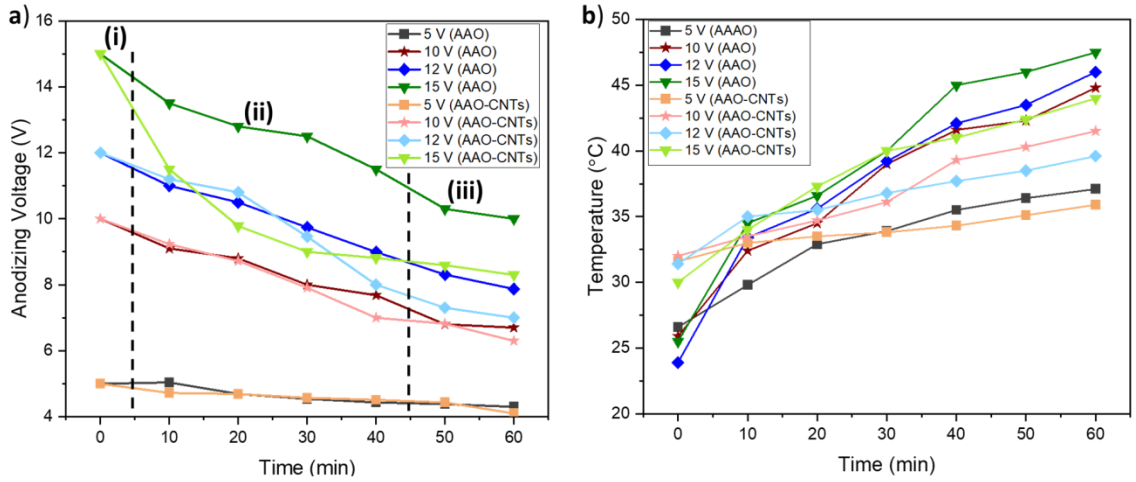

Figure 2: (a) Anodizing voltage and (b) Electrolyte temperature during the anodization.

The data also suggested that the anodization process is related to the growth mechanism of the AAO as depicted in Figure 3(a). From Figure 2(a), the mechanism can be compromised into three which are, (i) A linear decrease in voltage during the initial anodizing process, which indicates the growth of barrier layer on the Al surface, (ii) a slight decrease in voltage, representing the formation of composite oxide film through a selective dissolution of barrier oxide into acidic solution, and (iii) a steady-state phase where the AAO grow (Asadi et al., 2019). Mainly, the mechanism can be described according to the following chemical reaction:

For stage (i), the formation of a barrier layer takes place when Al^{3+} ions migrate from the AA2017 surface across the metal/oxide interface to create a thin barrier layer (Equation 1). The electrolysis of water occurrs from electrolyte forming O^{2-} ions and moving to the Al surface (Equation 2). It can be presented by:

$$Al \rightarrow Al^{3+} + 3e^{-} \quad (1)$$

$$2H_2O \rightarrow 2O^{2-} + 4H^{+} \quad (2)$$

From Figure 2(a)(i) above, it is suggested that during the initial process of anodization, the surface of Al alloy remains relatively smooth throughout the anodizing process. However, as Al^{3+} ions migrate and form the dense and compact barrier layer, a voltage drop occurred due to its development, as illustrated in Figure 3(a). The thickness of barrier oxide is directly proportional to the applied voltage (Kikuchi et al., 2015). During stage (ii), under the influence of an electric field, O^{2-} ions react with Al^{3+} ions forming Al_2O_3 (Equation 3):

$$2Al^{3+} + 3O^{2-} \rightarrow Al_2O_3 \quad (3)$$

With the increased growth time, Al^{3+} ions bring more opportunities in forming the growth of AAO oxide film. As the anodization process involves the exchange of ions, the simultaneous migration of ions including the escape of Al^{3+} and O^{2-} leads to the quick formation of films. Thus, this rapid migration creates unstable pores formation of the film. Higher voltage will lead to the formation of craters between the neighbouring pores as shown in Figure 3(a)(iii). This unstable formation resulted in a minor increase in resistance leading to a slight reduction or local maximum of the voltage. This observation is correlated with previous studies (Asadi et al., 2019; Ayuma et al., 2022). The temperature for AAO was also observed to have increments along the anodizing process due to chemical anodic dissolution in forming dense oxide films. During stage (iii), Figure 2(a) depicts the voltage was almost relatively constant and it reached its steady-state phase.

As a result, prolonged anodizing time showed that AAO exhibited more pores formation with larger craters on the surface and higher surface roughness which will be discussed later. The incorporation of CNTs into pores can aid the surface porosity which can be classified as self-diffusion and electrophoresis (Mohamad et al., 2020). The movement of CNTs into the pores is supported by the stirring process along with anodizing. The process of self-diffusion and electrophoresis are illustrated in Figure 3(b). During self-diffusion, CNTs tend to move away from higher-concentration regions to lower-concentration regions. This self-diffusion can help the uniformity of CNTs distribution and influence the CNTs to be incorporated within pores. As the anodizing process used the electric field, it also caused an electrophoresis effect where the electrical force resulted in the migration of CNTs particles to the Al surface (Ayuma et al., 2022; Mohamad et al., 2020).

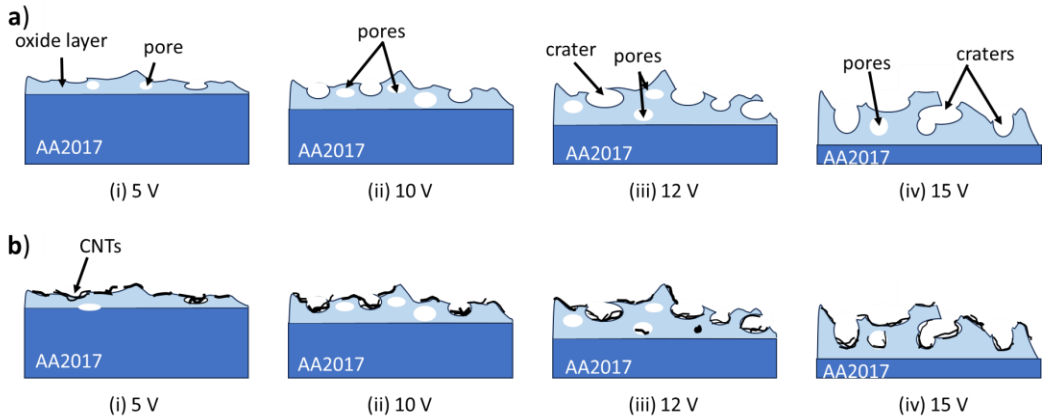

Figure 3: Growth mechanisms of: (a) AAO and (b) AAO-CNTs at different anodizing voltage.

3.2. Phase Composition Analysis

The effect of anodizing voltage on the phase composition analysis of AAO was determined by XRD analysis as shown in Figure 4. It shows the XRD patterns for the bare Al, AAO, and AAO-CNTS. The crystallite size, domain peak location, and FWHM are presented in Table 3.

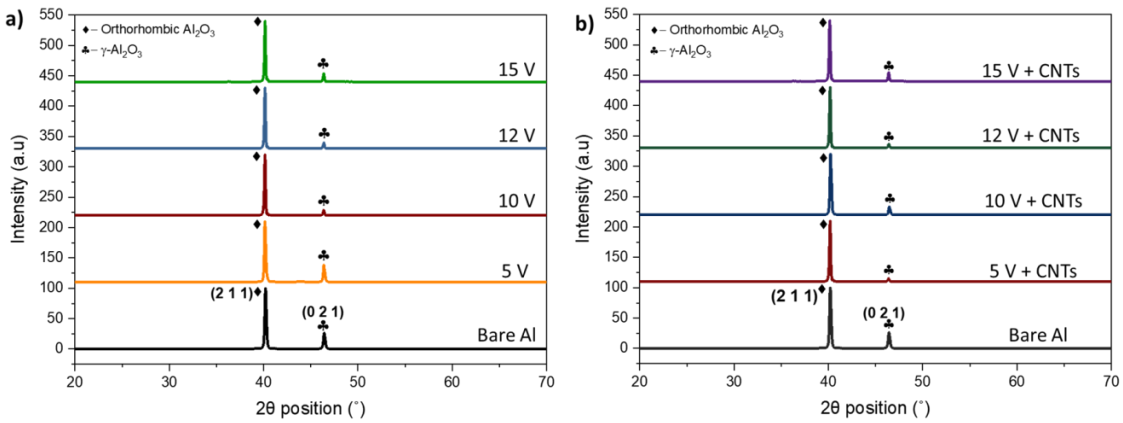

Figure 4: XRD pattern of anodizing voltage of (a) AAO and (b) AAO-CNTs.

The XRD patterns show peaks corresponding to orthorhombic Al_2O_3 (2 1 1)(JCPDS #98-010-2358) and γ-Al_2O_3 (0 2 1)(JCPDS #98-001-3124) crystallographic planes. It was identified that the coating formed on the Al substrate is composed of aluminium oxide with different crystallite structures as mentioned. The average crystallite size for bare Al in orthorhombic Al_2O_3 and γ-Al_2O_3 were determined using the Scherrer equation (Tollmien et al., 1961), with respective size of 213.61 nm and 72.76 nm. These calculated values depict the presence of a domain crystalline structure. Both planes experienced right shifting to higher 2θ which indicates Al crystal lattice strain in AAO. This shift is also evidence of the presence of finer grain size in AAO reinforced CNTs (Asadi et al., 2019). Due to the low amount (0.5 g/L) of CNTs, the XRD patterns do not exhibit carbon peaks of CNTs on the coated surface. Asadi et al. (2019) also proposed the same amount of 0.5 g/L MWCNTs in the Cu-MWCNTs composite, and the result showed there is no MWCNTs diffraction peak, owing to the low concentration of MWCNTs on the coated surface (Asadi et al., 2019).

Table 3: Phase information of the samples.

Plane	Sample	AAO					AAO-CNTs			
		0 V	5 V	10 V	12 V	15 V	5 V	10 V	12 V	15 V
(211)	Crystallite size (nm)	213.61	85.43	204.61	204.61	203.16	141.66	81.26	80.81	204.61
	Peak location (2θ)	40.18	40.13	40.15	40.15	40.15	38.49	40.22	40.18	40.15
	FWHM (°)	0.20	0.16	0.20	0.20	0.16	0.12	0.16	0.20	0.20
(021)	Crystallite size (nm)	72.76	36.37	36.37	72.75	87.30	36.15	218.30	218.27	72.75
	Peak location (2θ)	46.41	46.37	46.737	47.39	46.38	44.72	46.44	46.41	46.39
	FWHM (°)	0.20	0.20	0.20	0.20	0.20	0.16	0.20	0.20	0.16

3.3 Surface Topography

Pores dimension and surface roughness were further analysed using three-dimensional images (3D) of the optical profiler. Figures 5 and 6 displayed 3D images of AAO and AAO-CNTs formed at 60 minutes under different anodizing voltage using 5 V, 10 V, 12 V, and 15 V. The 3D images displayed a pattern of crests and troughs, which could be observed through the arrangement of different color regions ranging from blue to red. The profiler depicts detailed quantitative measurements regarding the analysis of surface characteristics such as surface roughness, R_a, and pores dimension (width and depth). The statistical graph obtained from the topographic analysis is presented in Figure 7. Figure 5(a) shows an even surface of bare Al with an approximate R_a value of 0.33 μm with the ground lines still can be seen on top of the surface. Based on referred anodizing voltage, R_a of AAO at 5 V, 10 V, 12 V, and 15 V are 0.80 ± 0.04 μm, 1.87 ± 0.01 μm, 3.40 ± 0.26 μm, and 5.71 ± 0.50 μm, respectively.

For AAO anodized under 5 V, Figure 5(b) depicted that the AAO had more roughness and an uneven appearance with multiple crests and troughs compared to the bare Al surface. It indicates the initial stage of anodizing as a result of Al^{3+} migration from Al alloy. Even so, AAO of 5 V was not enough to grow the porous structure as the ground lines were clearly visible on top of the Al surface. Prior to Figure 5(c, d, e), when the anodizing voltage was increased up to 15 V, the formed films presented a noticeable porous topography with many irregular peaks and shapes. Higher energy supplied indicates more bumps and rough surfaces, thus pores formation becomes more discernible. An increase in voltage leads to a formation of larger pore diameter and rate of adjacent pore nucleation (Li et al., 2014; Mahmud et al., 2015). This is due to higher anodizing voltage creating a more rapid formation of Al^{3+} and trapped O^{2-} to grow the oxide layer as discussed in Section 3.1. before. Due to the increased anodizing energy supplied, a thicker passive layer is created on the surface as a result of anodic oxidation (Gurgul et al., 2022).

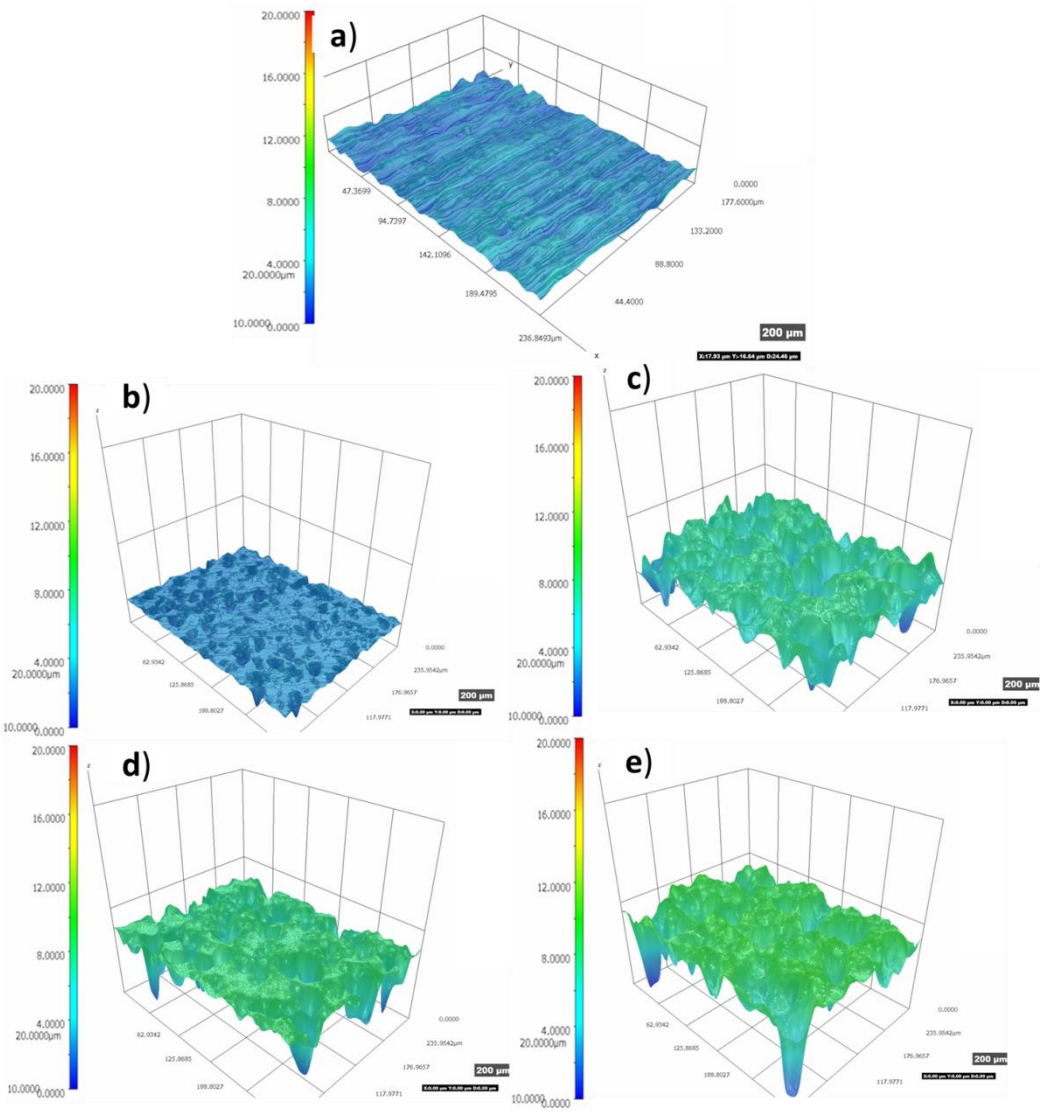

Figure 5: 3D image profiles of AAO with different anodizing voltage: a) bare Al alloy, b) 5 V, c) 10 V, d) 12 V and e) 15 V.

Generally, higher anodizing voltage increases the surface roughness of the AAO layer. This observation is correlated with previous works in which 15 V appeared to have surface roughness of 6.5 µm and 10.0 µm (Ayuma et al., 2022; Mohamad et al., 2020). It indicates that using energy supplied for 15 V was adequate to form a dense and thick oxide film. Besides calculating for Ra, the average width and depth of pores also take part to prove the dimension of pores. As seen in Figure 5(b, c) and Figure 7, there was a significant difference in width and depth concerning to 5 V and 10 V. A closer inspection of 10 V revealed the width and depth are 27.87 ± 2.45 µm and 19.26 ± 1.06 µm, hence resulted in more rough surface. The pores dimension of the surface after anodized using 12 V was determined to be approximately 30.09 ± 1.48 µm in width and 30.95 ±

1.67 μm in depth. On the other hand, for AAO anodized with 15 V, the measured width and depth of the pores were the highest, which are 43.69 ± 2.69 μm and 39.63 ± 1.64 μm, respectively. The results can be supported with SEM micrographs obtained from Figure 8, indicating the presence of numerous pores growth featured on the alloy's surface. Upon closer examination at higher magnification, the pores merged to form the large craters in the AAO. It can be concluded that anodization led to a gradual increase in surface roughness, along with the dimension of pores.

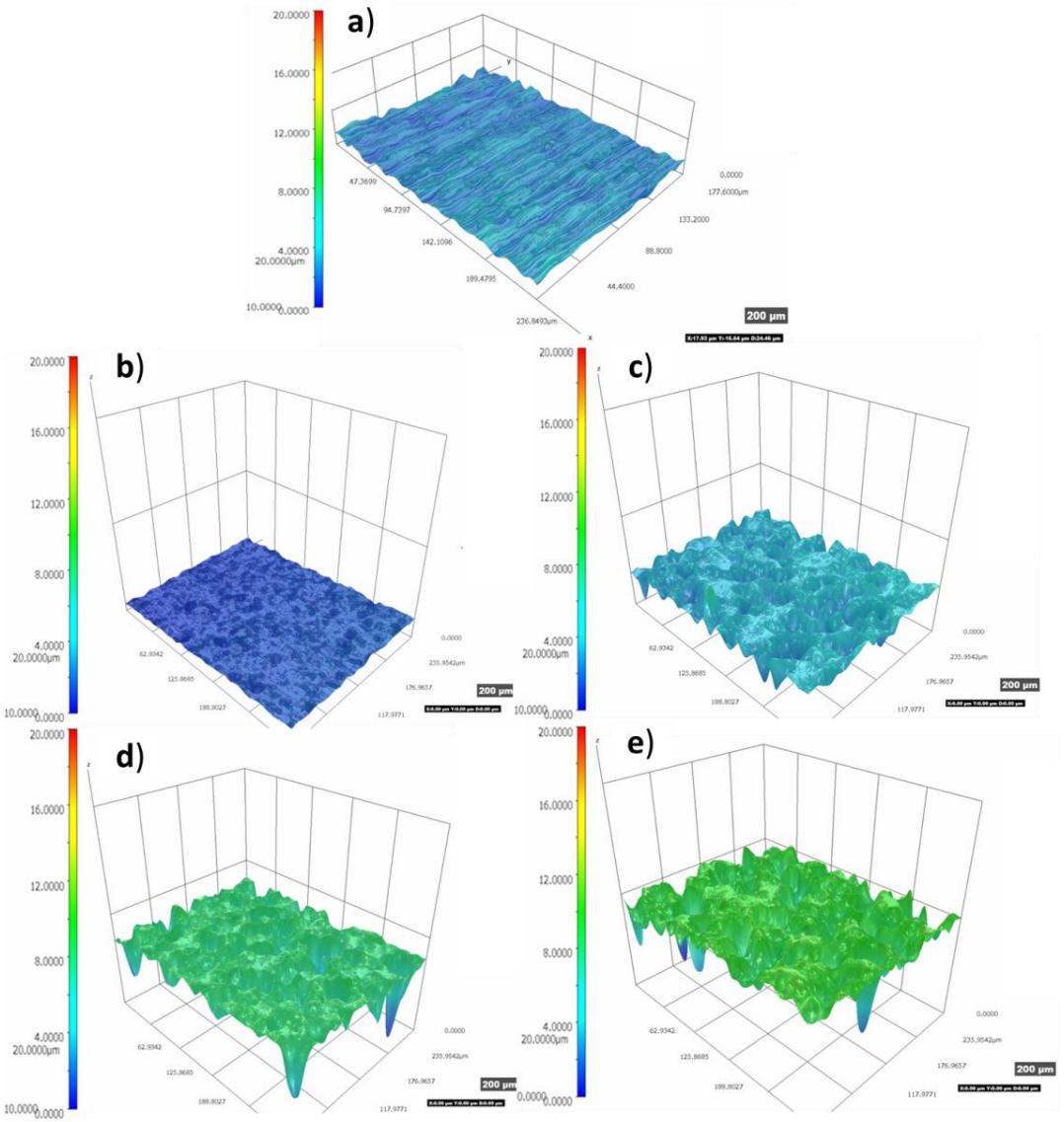

Figure 6: 3D image profiles of AAO-CNTs at different anodizing voltage: a) bare Al alloy, b) 5 V, c) 10 V, d) 12 V and e) 15 V.

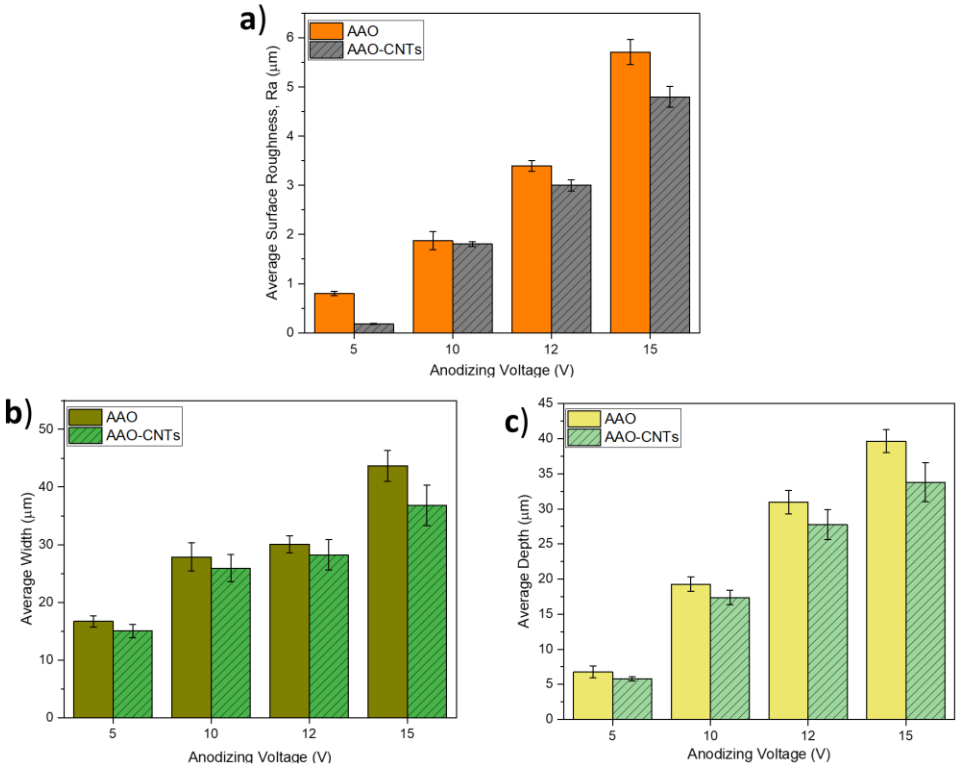

Figure 7: The analysis of surface topography of a) Average surface roughness, b) Average width, and c) Average depth of AAO and AAO-CNTs at different anodizing voltage.

In comparison with Figure 6, there were still irregular shapes and bumps on the alloy's surface, indicating the presence of a porous layer. Even so, the reinforcement of CNTs into AAO can improve the surface roughness and pores dimension. The introduction of CNTs into the Ni-P matrix resulted in a reduction of surface roughness by approximately 63%, decreasing it from 192 nm in the Ni-P coating to about 129 nm in the Ni-P-CNT composite (Alishahi et al., 2012). This is due to the electrophoresis effect by anodizing voltage that causes CNTs to move towards Al alloy. It can be proved from Figure 7, which revealed that CNTs content influenced the surface roughness and pores dimension. A lower anodizing voltage at 5 V prompts a slower electrochemical reaction, which causes the formation of pores to be relatively smaller. In contrast, at 10 V, the applied anodizing voltage is higher, thus causing an intense electrochemical reaction and accelerating the pore growth significantly. Regarding that, 10 V anodizing voltage brings more opportunities for a higher content of CNTs to embedded within the pores, resulting to a lower pore size and surface roughness compared to the AAO. Hence, the width of AAO-CNTs under 10 V, 12 V, and 15 V employed the values of 25.93 ± 2.35 µm, 28.22 ± 2.63 µm and 36.78 ± 3.53 µm, respectively. From quantitative measurement, it was found out that the highest average surface roughness of anodized AAO-CNTs was achieved under 15V anodizing voltage, specifically 4.80 ± 0.21 µm, respectively. This value represents approximately a 16% reduction compared to the surface roughness observed without CNTs reinforcement at the same 15 V anodizing voltage. It was followed by a reduction in surface roughness for 77%, 4%, and 12% in AAO-CNTs under 5

V, 10 V, and 12 V, respectively. It is suggested that CNTs has incorporated into the pores. Previous research by Gu et al. (2023) found out increasing the concentration of CNTs to 0.2 g/L leads to a more uniform coating on the surface, as CNTs influenced to reinforce into Ni-B-P composite coatings deposited on aluminium surface. Figure 7(b) and Figure 7(c) employed a significant reduction in average width and depth for all AAO-CNTs samples, as indicated by the graphs. The presence of MWCNTs had a significant impact on reducing both size and number of pores (Lee et al., 2011). As surface roughness decreased, the average width and depth also decreased.

3.4 Surface Morphology

Surface morphologies of AAO and AAO-CNTs are depicted in Figure 8. Both AAO and AAO-CNTs were formed using a voltage range from 5 V to 15 V for 60 minutes of anodizing time. At an initial anodizing voltage of 5 V, the size of irregular pores can be clearly observed as the pores started to form on the surface as seen in Figure 8(a). Many small pores were formed although the voltage supplied is low, which indicates that the anodizing process depends on anodizing voltage. Based on statistical measurement using ImageJ, the calculated porous area was 29.41 μm^2, respectively. The AAO formed at low voltage exhibits low quality arrangement (Stępniowski et al., 2012). However, 5 V supplied showed that the oxide films deposited on the Al surface did not exhibit uniform coverage, as the SEM image revealed that there were still lots of scratch line visible from the previous grinding. In contrast with Figure 8(b), it is inferred that CNTs were embedded into pores, which can be compromised with EDX analysis as shown in Figure 9. The porous area was determined to be 24.07 μm^2 and the value showed that the number of pores became lesser after filling in with reinforcement particles. It is correlated with previous discussions from Figure 7 showing that the effect of CNTs can reduce the surface porosity.

When extending the anodizing voltage up to 15 V, the number of pores formed tended to be larger in size and were seen to be much more prominent as seen in Figure 8(c). From ImageJ, it showed that the calculated porous area value was 937.65 μm^2, respectively. Due to that, larger craters can be observed on the alloy's surface due to the thickening of the oxide layer. The gradual increase in thickness of the porous layer results in the development of distinct crater-like structures (Gurgul et al., 2022). It is due to pores development in the oxide layer. The porous area of AAO-CNTs in Figure 8(d) exhibited lesser value compared to AAO anodized under 15 V which is 616.58 μm^2, respectively. In prior studies employing micro-arc oxidation in titanium alloy, high-magnification SEM examinations revealed a significant amount of CNT accumulation within the pores (Yazici et al., 2014). Figure 9 shows the SEM image with the element distribution of sample 15V of AAO-CNTs. The EDX element distribution is measured from the pore (location X) on the oxide surface, indicating 22.98 wt% of carbon element. Hence, it is suggested that CNTs embedded into the pores and minimize the size of pores.

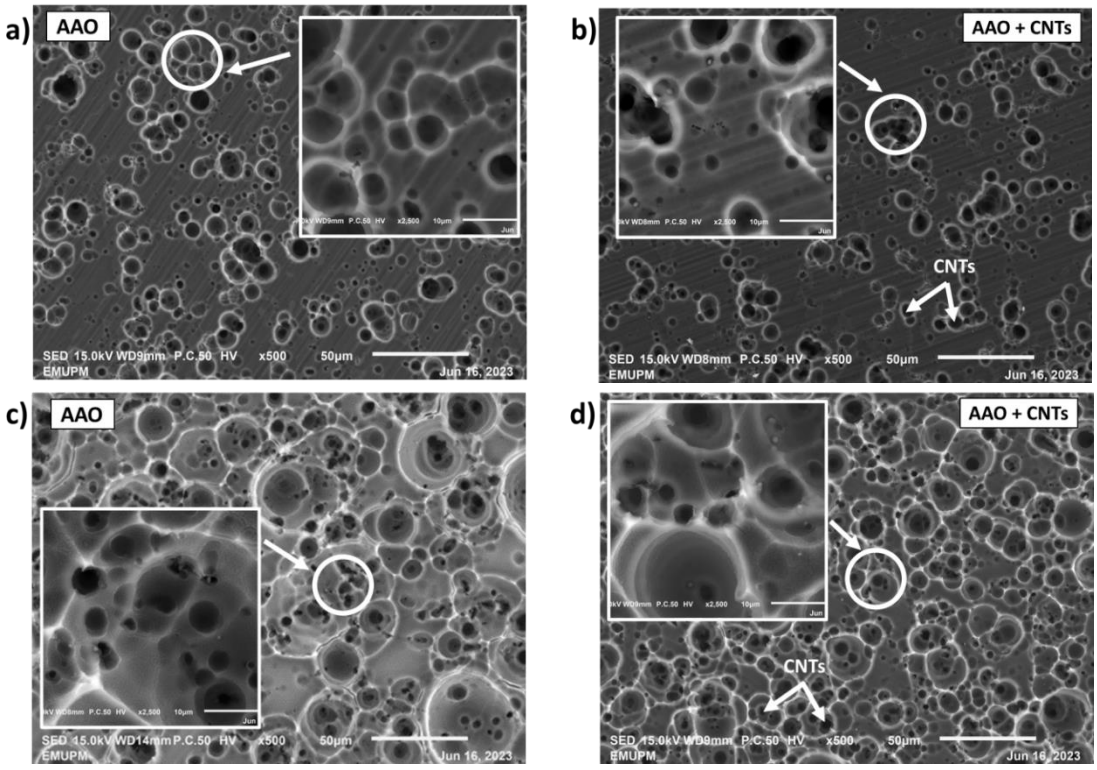

Figure 8: Surface morphologies of anodized samples at 5V and 15 V: (a-c) AAO and (b-d) AAO-CNTs.

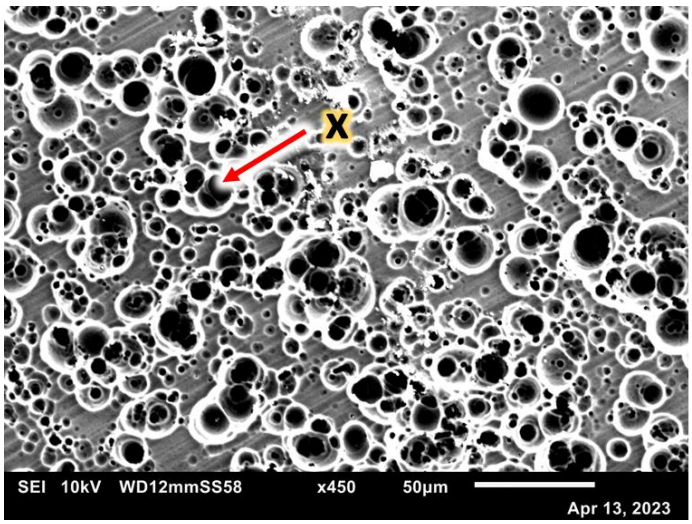

At point X,

Element Distribution (WT %)	
O	55.22
C	22.98
Al	21.80

Figure 9: SEM-EDX of AAO-CNTs at 15 V.

3.5 The Vickers Hardness

Figure 10 displays the analysis of microhardness results for bare Al alloy, AAO, and AAO-CNT at different anodizing voltage under 60 minutes. Based on observation, AAO anodized samples employed higher microhardness trends compared to bare Al alloy. Despite showing a promising increase in values for all anodized samples, the AAO under 5 V shows the lowest value which is 111.25 ± 10.46 HV, respectively. The findings suggested that under 5 V anodizing voltage, the anodization process is inadequate in fully converting the Al surface into a dense and stable oxide film. Consequently, numerous micro and nano pores remain on the surface as seen in Figure 8, which can adversely impact the microhardness of the oxide film. For AAO anodized under 10 V, 12 V, and 15 V, the samples exhibited lower microhardness. This is due to the presence of surface porosity that can lead to a reduction in surface strength and ductility of materials. The existence of pores and increment in porosity resulted in a decline of coating hardness (Dervishi et al., 2022). The hardness surpassed higher values when the composite oxide layer was reinforced with CNTs. The highest microhardness of 210.40 ± 2.80 HV was attained under the 15 V anodizing voltage of AAO-CNTs. It is suggested that the increment in microhardness graphs is due to the dispersion hardening effect by CNTs that can form strong interfacial bonding with the oxide matrix. CNTs serve as pathways or bridges that can transfer the force efficiently throughout the composite oxide film, thus strengthening the composite oxide layer. CNTs have the capacity to bridge the cracks within the coating, thus effectively impeding crack propagation in composite materials (Sabouri & Mousavi Khoei, 2018). The rise in microhardness can be attributed to the dispersion hardening effect induced by carbon nanotubes, which impedes dislocation movement in binary nickel coatings (Gul et al., 2023). This is in agreement with previous research where the microhardness value of CNTs reinforced in Al-alloy foams was found to be 93.43 HV, significantly surpassing 60 HV of non-reinforced Al-alloy (Duarte et al., 2015).

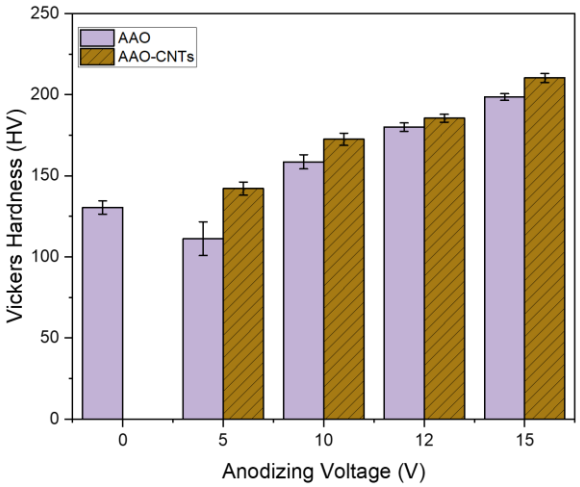

Figure 10: Microhardness of AAO and AAO-CNTs at different anodizing voltage.

CONCLUSIONS

In this paper, the AAO and AAO-CNTs were successfully synthesized through an anodizing technique. XRD result revealed that the peaks correspond to orthorhombic Al_2O_3 (2 1 1) and γ-Al_2O_3 (0 2 1) crystallographic planes. Besides that, an increase in voltage up to 15 V led to the highest surface roughness of AAO compared to bare Al alloy, approximately 5.71 ± 0.50 μm, with widths measuring around 43.69 ± 2.69 μm and depths of approximately 39.63 ± 1.64 μm. In contrast with AAO-CNTs, it showed an improvement in enhancing surface coverage and performance of composite oxide films by CNTs reinforcement. The findings of 3D images revealed that the surface roughness reduced to 4.80 ± 0.21 μm, along with a decrement in pores dimension. The surface hardness properties after being reinforced with CNTs also show enhancement. The improvement for bare Al alloy can be achieved, in which the highest hardness of AAO-CNTs is 210.40 ± 2.80 HV. This research shows promising results of AAO-CNTs as a potential candidate for protective coating applications in industrial machining and automotive applications.

ACKNOWLEDGMENTS

This research is supported by Malaysia Ministry of Higher Education (MoHE) under the Fundamental Research Grant Scheme (FRGS/1/2022/STG05/UPM/02/3) for the project number 5540572. I also thanks Mr Muhammad Bustami Bin A Razak from TriPrem i-Kohza, Malaysia-Japan International Institute of Technology, Universiti Teknologi Malaysia for his help.

REFERENCES

Alishahi, M., Monirvaghefi, S. M., Saatchi, A., & Hosseini, S. M. (2012). The effect of carbon nanotubes on the corrosion and tribological behavior of electroless Ni-P-CNT composite coating. Applied Surface Science, 258(7), 2439–2446.

Asadi, A., Pourfattah, F., Miklós, I., & Afrand, M. (2019). Ultrasonics - Sonochemistry E ff ect of sonication characteristics on stability, thermophysical properties, and heat transfer of nano fl uids: A comprehensive review. 58(February).

Ayuma, N., Tahir, M., Liza, S., Fukuda, K., Mohamad, S., Zakir, M., Hashimi, F., Saifulnizam, M., Yunus, M., Yaakob, Y., & Othman, I. S. (2022). Surface and Tribological Properties of Oxide Films on Aluminium Alloy through Fly-Ash Reinforcement.

Brudzisz, A. M., Giziński, D., & Stępniowski, W. J. (2021). Incorporation of ions into nanostructured anodic oxides—mechanism and functionalities. Molecules, 26(21).

Brzózka, A., Brudzisz, A., Rajska, D., Bogusz, J., Palowska, R., Wójcikiewicz, D., & Sulka, G. D. (2020). Recent trends in synthesis of nanoporous anodic aluminum oxides. In Nanostructured Anodic Metal Oxides: Synthesis and Applications. INC.

Chan, K.F., Zaid, M. H. M., Mamat, M. S., Liza, S., Tanemura, M., & Yaakob, Y. (2021). Recent developments in carbon nanotubes-reinforced ceramic matrix composites: A review on dispersion and densification techniques. Crystals, 11(5).

Da Silva Tousch, C., Magniez, L., Fontana, S., Marcos, G., Hérold, C., Henrion, G., Czerwiec, T., & Martin, J. (2023). Influence of carbon nanotubes on the plasma electrolytic oxidation process of aluminum under “soft” sparking conditions. Surface and Coatings Technology, 468(June).

Dervishi, E., McBride, M., Edwards, R., Gutierrez, M., Li, N., Buntyn, R., & Hooks, D. E. (2022a). Mechanical and tribological properties of anodic Al coatings as a function of anodizing conditions. Surface and Coatings Technology, 444(May), 128652.

Dervishi, E., McBride, M., Edwards, R., Gutierrez, M., Li, N., Buntyn, R., & Hooks, D. E. (2022b). Mechanical and tribological properties of anodic Al coatings as a function of anodizing conditions. Surface and Coatings Technology, 444(June), 128652.

Duarte, I., Ventura, E., & Olhero, S. (2015). An effective approach to reinforced closed-cell Al-alloy foams with multiwalled carbon nanotubes. 95, 589–600.

Ebhota, W. S., & Jen, T.-C. (2018). Intermetallics Formation and Their Effect on Mechanical Properties of Al-Si-X Alloys. In Intermetallic Compounds - Formation and Applications (Vol. 11, Issue tourism, p. 13). InTech.

Gul, H., Algul, H., Akyol, A., Uysal, M., & Alp, A. (2023). Evaluation of wear and corrosion behavior of electroless Ni-B-P/CNT composite coatings on aluminum surfaces. Diamond and Related Materials, 137(January), 110075.

Gurgul, M., Syrek, K., Kozieł, M., Pięta, Ł., & Zaraska, L. (2022). Electrochemical growth and characterization of micro/nanostructured SnOx with crater-like morphology. Electrochimica Acta, 423(March).

Hwang, M., & Chung, W. (2018). Effects of a carbon nanotube additive on the corrosion-resistance and heat-dissipation properties of plasma electrolytic oxidation on AZ31 magnesium alloy. Materials, 11(12).

Jagannatham, M., Sankaran, S., & Haridoss, P. (2015). Materials Science & Engineering A Microstructure and mechanical behavior of copper coated multiwall carbon nanotubes reinforced aluminum composites. Materials Science & Engineering A, 638, 197–207.

Jagannatham, M., Sankaran, S., & Prathap, H. (2015). Applied Surface Science Electroless nickel plating of arc discharge synthesized carbon nanotubes for metal matrix composites. Applied Surface Science, 324, 475–481.

Lee, K. M., Ko, Y. G., & Shin, D. H. (2011). Incorporation of multi-walled carbon nanotubes into the oxide layer on a 7075 Al alloy coated by plasma electrolytic oxidation: Coating structure and corrosion properties. Current Applied Physics, 11(4 SUPPL.), S55–S59.

Li, Q., Liang, J., Liu, B., Peng, Z., & Wang, Q. (2014). Effects of cathodic voltages on structure and wear resistance of plasma electrolytic oxidation coatings formed on aluminium alloy. Applied Surface Science, 297, 176–181.

Mahmud, A. H., Habiballah, A. S., & Jani, A. M. M. (2015). The effect of applied voltage and anodisation time on anodized aluminum oxide nanostructures. Materials Science Forum, 819(May), 103–108.

Mohamad, S., Liza, S., & Yaakob, Y. (2020). Surface & Coatings Technology Strengthening of the mechanical and tribological properties of composite oxide film formed on aluminum alloy with the addition of graphite. Surface & Coatings Technology, 403(September), 126435.

Naqi, A., Abbas, N., Zahra, N., Hussain, A., & Shabbir, S. Q. (2019). Effect of multi-walled carbon nanotubes (MWCNTs) on the strength development of cementitious materials. Journal of Materials Research and Technology, 8(1), 1203–1211.

Rawian, N. A. M., Akasaka, H., Liza, S., Fukuda, K., Zulkifli, N. A., Tahir, N. A. M., & Yaakob, Y. (2023). Surface and tribological characterization of anodic aluminum oxide coating containing diamond-like carbon flakes. Diamond and Related Materials, 132(September 2022), 109674.

Remešová, M., Tkachenko, S., Kvarda, D., Ročňáková, I., Gollas, B., Menelaou, M., Čelko, L., & Kaiser, J. (2020). Effects of anodizing conditions and the addition of Al2O3/PTFE particles on the microstructure and the mechanical properties of porous anodic coatings on the AA1050 aluminium alloy. Applied Surface Science, 513(February).

Sabouri, M., & Mousavi Khoei, S. M. (2018). Plasma electrolytic oxidation in the presence of

multiwall carbon nanotubes on aluminum substrate: Morphological and corrosion studies. Surface and Coatings Technology, 334(June 2017), 543–555.

Stêpniowski, W. J., Norek, M., Michalska-Domańska, M., Bombalska, A., Nowak-Stêpniowska, A., Kwaśny, M., & Bojar, Z. (2012). Fabrication of anodic aluminum oxide with incorporated chromate ions. Applied Surface Science, 259, 324–330.

Sulka, G. D. (2008). Highly Ordered Anodic Porous Alumina Formation by Self-Organized Anodizing. In Nanostructured Materials in Electrochemistry.

Tollmien, W., Schlichting, H., Görtler, H., & Riegels, F. W. (1961). Tragflügeltheorie. Ludwig Prandtl Gesammelte Abhandlungen, 346–372.

Yang, H., Li, Y., Qiu, J., Song, Z., Bi, G., & Zhou, H. (2022). Interfacial Characteristics of 6061/AZ31B Composites in Multi-Pass Rolling. Materials, 15(3), 1–16.

Yazici, S. K., Muhaffel, F., & Baydogan, M. (2014). Effect of incorporating carbon nanotubes into electrolyte on surface morphology of micro arc oxidized Cp-Ti. Applied Surface Science, 318, 10–

Zhang, D., Dong, G., Chen, Y., & Zeng, Q. (2014). Applied Surface Science Electrophoretic deposition of PTFE particles on porous anodic aluminum oxide film and its tribological properties. Applied Surface Science, 290, 466–474.

Zhang, T., Kumari, L., Du, G. H., Li, W. Z., Wang, Q. W., Balani, K., & Agarwal, A. (2009). Mechanical properties of carbon nanotube-alumina nanocomposites synthesized by chemical vapor deposition and spark plasma sintering. Composites Part A: Applied Science and Manufacturing, 40(1), 86–93.